

Influence of Layer Height on Thermal Buoyancy Convection in A System with Two Superposed Fluids Confined in A Parallelepipedic Cavity

Sunil Punjabi¹, K. Muralidhar², P. K. Panigrahi²

Abstract: Convection in a differentially heated two-layer system consisting of air and water was studied experimentally, using laser-interferometry. The cavity used for flow visualization was square in cross-section and rectangular in-plan having dimensions of $447 \times 32 \times 32$ mm³. Experiments performed over different layer thicknesses of water filled in a square cross-section cavity, the rest being air, are reported in the present work. The following temperature differences for each layer height were imposed across the hot and the cold walls of the superposed fluid layers: (i) $\Delta T=10$ K and (ii) $\Delta T=18$ K. The present study was aimed at understanding the following issues: (a) the influence of Rayleigh number on the steady thermal field, and (b) flow coupling mechanisms between the layers. Experiments show that the thermal field in the fluid layers is primarily determined by the temperature difference and hence the Rayleigh number. In the thicker water layer (1/3 air - 2/3 water) case, with increase in Rayleigh number, the no-coupling mode changes into a thermal coupling mode. For the equal layer heights (1/2 air - 1/2 water) case, the two-layers are thermally coupled at a lower Rayleigh number, while the mechanical and thermal coupling both become significant at higher Rayleigh number. Also, for the thicker air layer (2/3 air - 1/3 water) case, a full or joint coupling (mechanical + thermal) was observed for all the Rayleigh numbers obtained in the experiment.

keyword: Convection, Superimposed fluid layers, Rayleigh number, Air-water interface, Flow coupling, Interferometry.

Nomenclature

A aspect ratio, L/H
g acceleration due to gravity, m.s⁻²

h height of the fluid layer, m
 H height of the cavity, m
 L length of the cavity, m
 n refractive index of the fluid
 n_o reference value of refractive index
 dn/dT refractive index change with temperature, K⁻¹
Nu Nusselt number, $(-H/\Delta T) (\partial T/\partial y)|_{y=0,H}$
Pr Prandtl number, ν/α
Ra Rayleigh number, $\frac{g\beta(T_{hot}-T_{cold})h^3}{\nu\alpha}$
 T temperature, °C
 T_{hot} temperature of the bottom hot wall, °C
 T_{cold} temperature of the top cold wall, °C
 T_I interface temperature, °C
 W width of the cavity, m
 y/H non-dimensional vertical coordinate, measured from the average interface position

Greek Symbol

α thermal diffusivity, m².s⁻¹
 β coefficient of thermal expansion, K⁻¹
 λ wavelength of the laser, nm
 ν kinematic viscosity, m².s⁻¹
 ρ fluid density, kg.m⁻³
 σ surface tension, N.m⁻¹
 $\frac{d\sigma}{dT}$ surface tension gradient with respect to temperature, N/m-K
 θ nondimensional temperature, $\frac{(T-T_{cold})}{(T_{hot}-T_{cold})}$
 ΔT temperature difference across the cavity, $(T_{hot}-T_{cold})$, K
 ΔT_ε temperature difference between successive fringes, K

1 Introduction

Convection refers to heat transfer in a fluid when enhanced by energy transport due to fluid velocity. In natural convection, fluid motion is set up solely by the buoy-

¹ Corresponding Author: Post-doc fellow, School of Mechanical Engg., Tel Aviv University, 69978 Tel Aviv Israel. E-mail: sunil@eng.tau.ac.il.

² Department of Mechanical Engineering, Indian Institute of Technology (I.I.T), Kanpur 208016 India

ancy forces arising from the presence of differentially heated boundaries.

Rayleigh-Benard convection refers to the flow field in a fluid layer that is confined between two parallel infinite thermally conducting plates, and is heated from below and cooled from above. The motion is driven by a fixed temperature difference. The hot fluid expands and produces an unstable density gradient in the fluid layer. If the density gradient is sufficiently strong, the hot fluid rises and the cold fluid descends, thus setting up a roll pattern. The convective flow results in an enhanced heat transport from the hot to the cold surface.

In single layer convection, a fluid completely fills the space between the plates and no free surface is formed. Convective motion starts once the buoyancy force exceeds the viscous force. The relative strength of the two forces is characterized by a dimensionless quantity, the Rayleigh number (Ra). It is the relative measure of the potential energy available in the buoyancy field to viscous dissipation. The non-dimensional parameter Rayleigh number Ra is defined in terms of buoyancy and viscous forces as

$$Ra = \frac{\text{gravitational potential energy}}{\text{viscous dissipation}} = \frac{g\beta(T_{hot} - T_{cold})h^3}{\nu\alpha} \quad (1)$$

Two-layer convection refers to buoyancy-driven movement in differentially heated superposed horizontal fluid layers. The main difference between one and two layer convection is in the appearance of an interface (a free surface if one of the fluids is a gas). Convection in such problems can be surface tension driven, in addition to being supported by buoyancy.

In a two-layer system, Rayleigh-Benard convection is characterized by two distinct modes of flow coupling between the fluid phases, *via* the interface. These are respectively known as thermal coupling and mechanical coupling (viscous coupling). In thermal coupling, the recirculation patterns in the individual layers are driven by the temperature difference appropriate for each of them. It is thus possible for the rolls in each phase to have identical sense, clockwise or anti-clockwise. In mechanical coupling, the circulation in one phase drives that in the other by the mechanism of viscosity, thus requiring that the the two rolls be oppositely oriented.

The configuration of interest in the present work has fun-

damental as well as practical importance. Applications of two-layer convection can be seen in large scale geophysical studies and classified technologies such as crystal growth.

Zeren and Reynolds (1972) conducted analytical studies on a two-layer system and predicted that the stability limits are dependent on the properties of the fluids. Instability was also seen to vary with the total depth of the layer and the ratio of the layer heights. Rasenat, Busse and Rehberg (1989) developed a mathematical model to investigate the onset of convection in two layers of immiscible fluids. Two superposed fluids with combinations of ethylene glycol-oil and ethylene glycol-decane were selected. The authors showed that the convection in the two layers may occur in the form of either viscously or thermally coupled motions. Dijkstra (1992) numerically studied pattern selection in small aspect ratio containers. The author concluded that the no-slip side-walls greatly influence the multiplicity of stable steady patterns. Prakash and Koster (1996) have experimentally studied two-dimension convection in a system of two immiscible liquids. For flow visualization, real-time holographic interferometry was used. The authors concluded that thermal and mechanical coupling mechanisms are possible between the fluid layers, depending on the fluid properties and the cavity Rayleigh number. Andereck, Colovas and Peter (1996) presented experimental results for two immiscible fluid layers, driven by a vertical temperature gradient. They observed time dependent variations in the nature of coupling between the two layers. Schatz, VanHook, McCormick, Swift and Swinney (1999) worked with a two-layer system consisting of silicone oil (Pr=81) and air. The shadowgraph technique was used for flow visualization. The authors reported on the transition between hexagonal and square patterns in the convection planforms. It was concluded that the transition occurs as the heating rate is increased. Johnson, Narayanan and Dauby (1999) have conducted experiments to study the effect of layer height on the pattern formation in silicone oil-air system (for flow visualization an inframetric camera was used; the camera measures the infrared radiation emitted by silicone oil and thus determines the temperature distribution at the interface). Mishra, Muralidhar and Munshi (1999) addressed the problem of Rayleigh-Benard convection in a horizontal single layer of air at a Ra=34,800. The authors interpreted their results to show that the flow in the fluid layer

is associated with a buoyant plume rising from the hot surface. The fluid was seen to be cooled at the top boundary while descending all around the central plume. Lappa (2005) in a recent numerical study conducted in closed and open parallelepipedic and cubical containers investigated the influence of both buoyancy and surface tension forces under different heating conditions. Stable and unstable flow regimes in the cavities filled with silicon melt ($Pr = 0.01$) were obtained using non-linear balance equations through multiprocessor computations. The author concluded that numerical simulations may help in validating new and complex models and also could provide a more adequate scientific foundation in understanding industrial processes. In another recent numerical study, Mosaad, Nakhi and Al-Hajeri (2005) reported a complex conjugate convection problem that deals with the thermal interaction between two fluid media (undergoing free and forced convection) at two different bulk temperatures and separated by a plate that acts as a diathermic wall. The authors estimated the mean conjugate Nusselt number over the entire plate extension as a function of controlling parameters.

The fluid phases considered in the present work are air and water. Experiments have been conducted over different layer heights of fluids, and with increasing values of the cavity temperature differences, for each height combination. The convection pattern in the cavity has been imaged using a laser interferometer. The objectives of the present work are to examine the influence of Rayleigh number on the steady thermal field, temperatures attained at the interface, heat fluxes at the solid walls in terms of Nusselt number (Nu), and the nature of flow coupling between the two horizontal layers. An order-of-magnitude analysis showed surface tension effects to be of secondary importance in the present work. This was demonstrated for an octagonal cavity consisting of similar fluid layers (Punjabi, Muralidhar and Panigrahi (2004)).

2 Apparatus and Instrumentation

The test cell consists of three sections namely the top tank, the test section and the bottom tank. Fig. 1 shows the schematic diagram of the test-cell. The cavity has a square cross-section of edge 32 mm and a length of 447 mm, thus giving an aspect ratio of around 14. To a first approximation, this represents a near two dimensional cavity in the sense that gradients are dominant in the ver-

tical direction, but not along the cavity length. The two dimensional approximation of the thermal field is known to be unrealistic at very high Rayleigh numbers (Mishra, Muralidhar and Munshi, 1999). The fluid layer is confined by two aluminium plates of thickness 3 mm above and below to provide isothermal conditions. The two longer side walls are made of perspex and bakelite sheets which act as insulating walls. The two square sides are covered by optical windows to permit the passage of the light beam. The windows are made of fused silica, since it has excellent surface properties such as parallelism, transparency and surface finish. The horizontal hot and the cold surfaces have been maintained at uniform temperatures by circulating water continuously over them from constant temperature baths (RAAGA and HUBER). In a model experiment, the top wall is cooled to 16°C , while the bottom wall is heated to 26°C , the ambient temperature being 22°C . Both walls have been maintained at the respective temperatures to within $\pm 0.05^{\circ}\text{C}$ during the experiments. The temperature difference across the cavity for this experiment is 10 K, with a tolerance of $\pm 0.05^{\circ}\text{C}$. In another experiment, a temperature difference of 18 K across the cavity was maintained. All experiments have been continued for 6-8 hours to confirm that a steady state was reached in the fluid layers. Although, the flow field gets nominally stabilized in 2-4 hours, the experiment was continued for additional 2-4 hours for detecting changes in the fringe field. As the volume of the test-cell is small, the thermal fields in the hot and the cold surfaces and the flow fields in the fluid layers all approach the steady state together. In this respect, the thermal loading of the two-layer system may be categorized as continuous, as against a sudden loading commonly employed in numerical calculations.

For the temperature field measurement in the fluid medium, the primary instrument employed is the Mach-Zehnder interferometer. It employs a 35 mW He-Ne laser and 150 mm diameter optics. Interferograms are recorded using a CCD camera with a 512×512 pixel resolution. The camera is interfaced with a PC through an 8-bit A/D card which digitizes light intensity levels over range of 0-255. Image acquisition is at video rates (50 images/s). Fig. 2 shows the experimental apparatus and instrumentation utilized in the present work.

For measurements in liquids a reference chamber is required to be included with the interferometer to compensate for refractive changes under isothermal conditions.

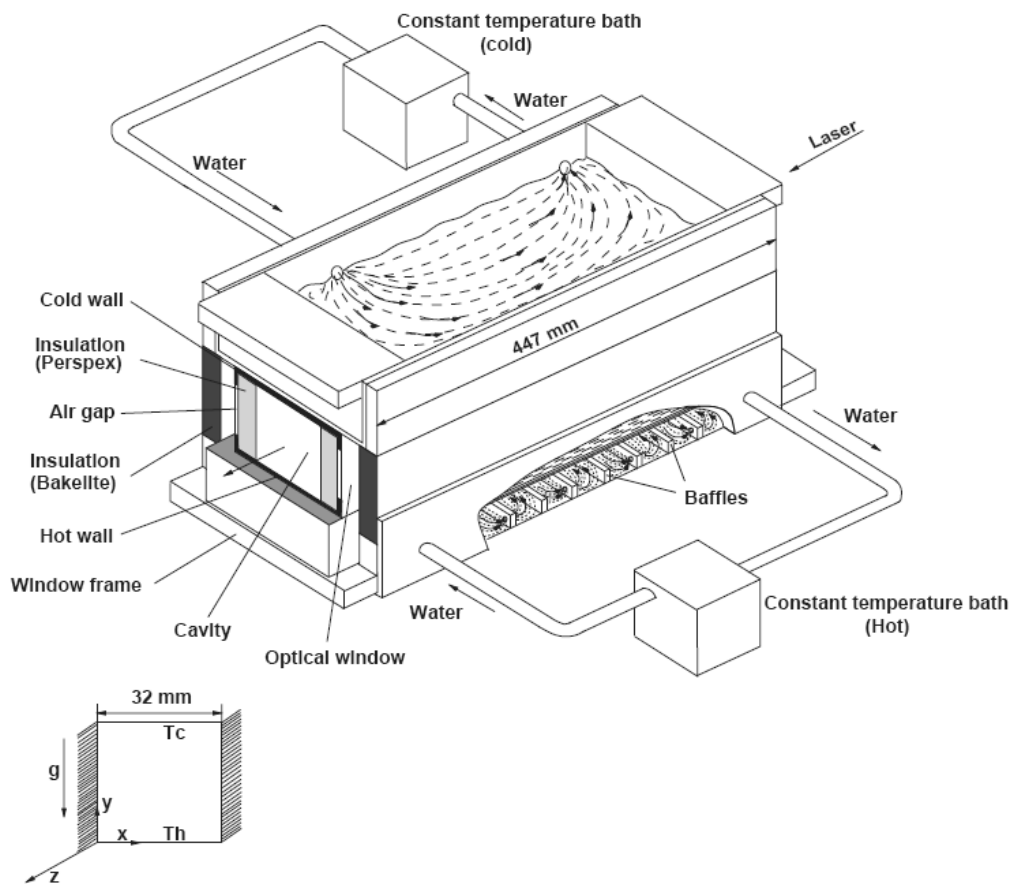


Figure 1 : Schematic drawing of the test-cell.



Figure 2 : Picture of the Experimental apparatus.

K-type thermocouples (24 gage) were used to monitor the temperature of the surfaces of the cavity and the ambient temperature throughout the experiment. They were connected to a 30 channel recorder (SAN-EI). All the experiments have been performed in the infinite fringe setting of the interferometer. When a thermal disturbance

is introduced in the path of the test beam, fringes appear in the field-of-view; that represent isotherms. The alignment of the interferometer in the infinite fringe setting was individually carried out to capture interferograms for the air and the water sides. For this purpose, the reference chamber was also filled with different thicknesses of water, the rest being air at atmospheric pressure. The temperature drop per fringe shift, ΔT_ϵ can be calculated from first principles of Goldstein (1983) as:

$$\Delta T_\epsilon = \frac{\lambda/L}{dn/dT} \tag{2}$$

where λ is the wavelength of laser beam, dn/dT is the rate of change of refractive index with temperature and L is the effective length of the test cell.

3 Data Reduction and Uncertainty Analysis

The methodology adopted in the present work is based on the analysis of the image (interferogram) obtained

from experiments. The image invariably contains superimposed noise. Image processing operations comprising of (a) filtering, (b) image enhancement, and (c) thinning were adopted, to remove the noise as well as to improve the quality of the image. Filtering utilizes the fast Fourier transform (FFT) algorithm to remove noise and retains information in the image. Image enhancement technique is subsequently required to improve the quality of the image that has become blurred owing to loss of contrast after filtering. Fringe thinning is a process of extraction of minimum intensities in the dark fringe bands. Calculations for the local and the average Nusselt number, and the temperature distribution have been accomplished using the thinned fringes of the interferogram.

Errors in the experimental data are associated with misalignment of the apparatus with respect to the light beam, image processing operations including filtering, thinning and assigning temperature of fringes. Errors related to refraction effects in case of water were found to be high and affected the air-water interface location. All experiments were conducted several times to establish the repeatability of the fringe patterns. The average Nusselt number of the cavity on the water and the air side were compared to those reported for single layer convection. For all experiments, the plate-averaged Nusselt number has been found to be in good agreement with published correlations. Interface temperatures calculated from the top and the bottom surfaces were within $\pm 4\%$. Uncertainty in comparison is expected since in a single fluid layer the top and bottom boundaries are solid walls, while in the present case, one of the boundary is an interface. For the air side, the Nusselt number matched the correlation to within $\pm 5\%$ and on water side it was within $\pm 16\%$. Comparison of Interface temperature and width averaged Nusselt Number with the reference values have been respectively summarized in Tab. 1 and Tab. 2. The Nusselt number correlations employed in the present work are given in Equations 4 and 5 in the following section.

4 Results and Discussion

As explained before, experiments were conducted in a two-layer system consisting of air present above water, both contained inside the rectangular in-plan (square cross-section) cavity. The following layer thicknesses of water filled in a cavity, the rest being air, have been selected for the experiments: (1) 1/3rd Air - 2/3rd Water, (2) 1/2 Air - 1/2 Water, and (3) 2/3rd Air-1/3rd Water.

The temperature differences imposed between horizontal hot (bottom) and cold (top) sides for each layer thickness for the experiments were: (i) $\Delta T=10K$ and (ii) $\Delta T=18K$. The results obtained from experiments are in the form of fringe patterns that are representative of buoyancy-driven flows in the two fluid phases. If the field is two dimensional, the fringes represent isotherms (constant temperature contours) owing to the infinite fringe setting of the interferometer. In three dimensions, the fringe patterns are indicative of the line integrals of the thermal field (Mishra, Muralidhar and Munshi, 1999).

Results are presented in terms of the interferometric images that depict the flow regimes established in the individual fluid phases (air and water) based on their respective Rayleigh numbers. The Rayleigh numbers in turn depends upon the temperature difference between the cold wall and the interface for the air phase; the hot wall and the interface for the water phase. Local as well as the average Nusselt numbers on the hot and the cold walls have been calculated to understand the energy transfer mechanisms at these locations. These are supplemented by the plots of the temperature distribution along the coordinate parallel to the height of the cavity.

The wall heat transfer rates have been determined in terms of the Nusselt number as

$$Nu = \left(-H/\Delta T \right) \left(\partial T / \partial y \right) |_{y=0,H} \quad (3)$$

where H is the height of the cavity. The average Nusselt number for each of the plates has also been compared with the experimental correlation for single fluid layer reported by Gebhart, Jaluria, Mahajan and Sammakia (1988). For air, the correlation is given by:

$$Nu(air) = 1 + 1.44 \left[1 - \frac{1708}{Ra} \right] + \left[\left(\frac{Ra}{5830} \right)^{1/3} - 1 \right] \quad (4)$$

For water, the correlation is given by:

$$Nu(water) = 1 + 1.44 \left[1 - \frac{1708}{Ra} \right] + \left[\left(\frac{Ra}{5830} \right)^{1/3} - 1 \right] + 2 \frac{(Ra)^{1/3}}{140} \left[1 - \ln \frac{(Ra)^{1/3}}{140} \right] \quad (5)$$

Results have been interpreted to understand the flow coupling mechanism, a special feature of two-layer convection. The coupling has been classified as thermal or me-

chanical depending on the sign of the respective rolls in the air and the water phases.

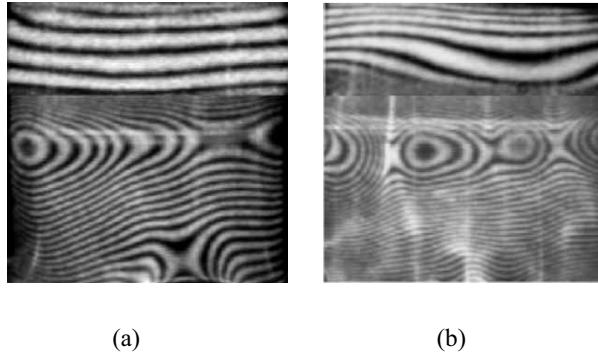


Figure 3 : Steady state interferogram for air-water system having a thick water layer in a square cross-section cavity with a temperature difference of (a) 10 K and (b) 18 K across the cavity.

4.1 Flow Characteristics in a Cavity - Thicker Water Layer

In the present set of experiments, the temperature differences of 10 K, and 18 K were imposed between the bottom (hot) and the top (cold) walls. The flow characteristics obtained in the two-layers are discussed below for each temperature difference.

In the first case ($\Delta T = 10$ K) the temperatures of the bounding hot and cold surfaces were maintained constant at 26 and 16° C. This corresponds to a cavity average temperature of 21° C. Using energy balance principles, it is possible to estimate the interface temperature by using the correlations Equations 4 and 5. The interface temperature for the present experiment thus has been found to be 25.80° C. The Rayleigh number in air and water layers can now be calculated to be 1,242 and 35,727 respectively. This indicates that the driving buoyancy potential in the water layer is around 29 times larger than in air. It is also to be noted that these Rayleigh numbers fall in the stable regime of the transition diagram discussed by Krishnamurti (1970). Accordingly, one can expect the thermal fields in the fluid layer to be two-dimensional. In the experiments, it was observed that convection develops in the lower water layer, due to a higher Rayleigh number as compared to the upper air layer. The interferogram depicted in Fig. 3(a) shows steady two-dimensional flow patterns in the two layer system. The fringes in

the water phase can be seen to be dense, even though the overall temperature difference taking place here is quite small. This is because the temperature drop per fringe shift (ΔT_ϵ) is much smaller for water as compared to air, the values being 0.016 and 1.527 K respectively. The higher Rayleigh number in water also indicates a more vigorous buoyant motion. This is confirmed by the greater displacement of the fringes, while those in air are almost straight. The interferogram in Fig. 3(a) has been captured after an experimental run time of 6 hours, when the flow field was fully evolved and the fringe patterns were quite steady. Since each fringe is an isotherm, regions of small fringe spacing can be associated with a large local diffusive heat flux.

In the portion of the cavity filled with air, in particular, a no-flow condition exists, as the Rayleigh number falls below the critical Rayleigh number value of 1708. It indicates that the buoyancy forces are not large enough to overcome the viscous forces to initiate convection in the air phase. The isotherms are equally spaced having negligible curvature due to the complete dominance of diffusive heat transfer. In the water phase, the largest local heat flux at the lower cavity wall at steady state occurs near the mid-plane of the cavity. Here, the flow develops in the form of two counter-rotating rolls with flow descending along the vertical axis close to the cavity center. The roll formed on the left side near the interface is quite strong as compared to that on the right side. The recirculating flow in water exhibits a strong convection, as seen in the greater curvature of the fringe patterns. The isotherms are denser near the lower hot wall and interface in comparison to the central region. This is because of the influence of diffusive heat transfer near the wall and interface in comparison to convection close to the central region. Dense fringes near the interface indicate the free surface to be thermally active, despite being a non-solid wall. The width averaged temperature profiles in the air and water sides of the cavity at steady state are shown in the upper-half of Fig. 6. The figure clearly indicates the large temperature drop on the air side as compared to the water side. Fig. 6 also shows the large temperature gradient near the cold wall due to the high density fringes near that region. Interface temperatures were calculated individually from the top as well as bottom walls. The thinned fringes for air and water were employed for this purpose. The temperature of each fringe is assigned on the basis of the value of ΔT_ϵ , Equation

2. The experimentally determined interface temperature was 25.72°C , while the value determined from correlations was 25.80°C . Thus the difference in the average value of the interface temperature between theory and experiment is less than $\pm 1\%$. This is shown in Tab. 1. Using the temperature profiles in the fluid layers, the local Nusselt number distribution was calculated at the hot and the cold walls of the cavity. The width averaged Nusselt number calculated on the basis of local Nusselt number are 0.98 and 3.21 for the top and the bottom walls respectively. The reference values given by [3] are 1.0 and 4.35 respectively in air and water. It is to be recalled that the correlation for the average Nusselt number considers a single layer in a cavity bounded by solid walls at top and bottom, unlike the present case, which has an interface. With this factor taken into account, it can be concluded that the Nusselt number in the present experiment is in good agreement with the reference correlation as shown in Tab. 2. The presence of a convective field in the fluid layers leads to a coupling between them. In the present case, due to the absence of convective flow in the air phase, the two-layers are not coupled in terms of flow at the interface.

In the second case, a temperature difference of 18 K was imposed between the surfaces having constant bounding temperatures of 34 and 16°C respectively for the hot (bottom) and cold (top) walls. The average cavity temperature was 25°C and the interface temperature was found to be 33.65°C . Accordingly, the Rayleigh number calculated in air and water are 2,100 and 98,505 respectively. This gives an extremely high driving buoyancy potential in water as compared to air. The flow in the water portion showed remarkable unsteadiness, unlike the air portion; where the flow was quite steady. It was observed that the flow in water reached the Time Dependent regime as discussed by Krishnamurti (1970). The fringe patterns in water were seen to switch among 9-10 states in the central portion of the cavity. The dominant mode after 6 hours of experimentation was recorded by the camera and is shown in Fig. 3(b).

In the air portion of the cavity, the flow develops in the form of a single roll which rises along the left side wall and descends along the right side wall. This gives a unicellular pattern in the cavity with sense of rotation in the clockwise direction. In the water phase, the flow develops in the form of six counter-rotating rolls with down-flow along the vertical axis close to the cavity cen-

ter and up-flow near the sides. A strong convective flow with high unsteadiness was registered in the central portion, while the fringe patterns near the hot wall attained a quasi-steady state. The temperature profiles of isotherms in the air and water sides of the cavity are shown in the lower-half of Fig. 6. The figure shows a larger temperature drop in air than in water. The interface temperature obtained from the experiments and its correlated values are shown in Tab. 1. The width averaged Nusselt Number obtained from the experiment and the reference values from correlation are summarized in Tab. 2. The differences in the Nusselt number calculated in the water phase have become larger. It may be due to the increased unsteadiness in the central portion that leads to some unsteadiness near the hot bottom wall. Flow coupling exists in the present experiment due to convective flow in both the layers. Here, a single roll in air, and six counter-rotating rolls in water have been observed. Convective flow in each layer is driven by the individual temperature differences across the respective fluid layers, indicating thermal coupling at the interface. Thus, we conclude that the thermal coupling exists inside the cavity at the interface.

4.2 Flow Characteristics in a Cavity - Equal Layer Heights

In the first case, a temperature difference of 10 K was imposed between the lower and the upper surfaces. This corresponds to a cavity average temperature of 21°C . The interface temperature for the present experiment has been found to be 25.79°C . The Rayleigh number in air and water layers have been calculated to be 4,185 and 16,413 respectively. This indicates that the driving buoyancy potential in the water layer is around 4 times larger than in air. The higher Rayleigh number in water also indicates a more vigorous buoyant motion. This is confirmed by the greater displacement of the fringes, while those in air are sensibly straight. This is shown in the interferogram of Fig. 4(a).

In the portion of the cavity filled with air, the largest local heat flux at the cooled cavity wall at steady state occurs at around the mid-plane of the cavity. The flow develops in the form of single roll which rises along the left side wall and descends along the right side wall. This gives a unicellular pattern in the cavity with a sense of rotation in the clockwise direction. The strength of convection in air is weak, as can be confirmed by the weak curvature

in the fringe patterns. The isotherms are densely placed near the top wall (the cold plate) as well as the interface in comparison to the central core region. The reason for this behaviour is the dominance of diffusive heat transfer near the walls. Near the interface the dense fringes indicate that the zone is thermally active, despite the fact that the water layer is not strictly a solid surface.

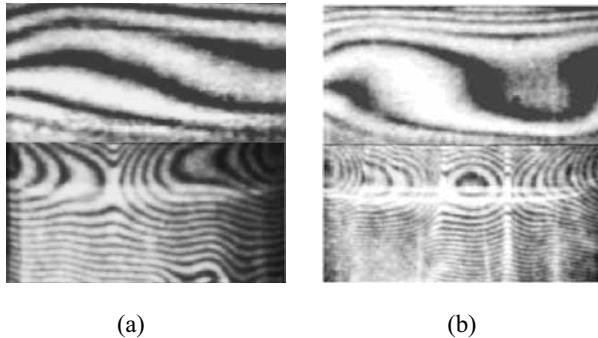


Figure 4 : Steady state interferogram for air-water system having equal layers heights in a square cross-section cavity with a temperature difference of (a) 10 K and (b) 18 K across the cavity.

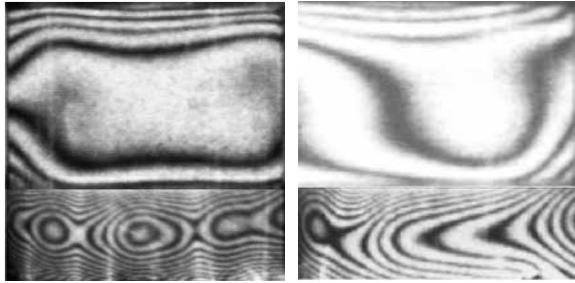
In the water phase, the largest local heat flux at the lower cavity wall at steady state occurs near the mid-plane of the cavity. Here the flow develops in the form of two counter-rotating rolls with flow descending along the vertical axis close to the cavity center. The recirculating flow in water exhibits stronger convection compared to air, as seen in the greater curvature of the fringe patterns. The isotherms are denser near the lower hot wall in comparison to the region near the interface. The temperature profiles in the air and water sides of the cavity at steady state are shown in Fig. 6. The figure clearly indicates the large temperature drop on the air side as compared to the water side. The experimentally determined interface temperature and the value determined from correlations are given in Tab. 1. The experimental and the reference width averaged Nusselt number are shown in Tab. 2. It is to be recalled that the correlation for the average Nusselt number considers single layer in a cavity bounded by solid walls at top and bottom, unlike the present case, which has an interface. The presence of a convective field in the fluid layers leads to a coupling between them; one may conclude that the two-layers are thermally coupled. In the second case, a temperature difference of 18 K was imposed between the two surfaces. The cavity average

temperature was 25°C. The interface temperature was calculated to be 33.64°C. The Rayleigh numbers were determined in the air and the water layers to be 7,088 and 42,147 respectively. This reveals that the driving buoyancy potential in the water layer is 6 times larger than in air. A high Rayleigh number in water was seen to develop a high unsteadiness in the fringe patterns of the water layer, particularly in the central region of the cavity. It was observed that the air layer also registered unsteady flow patterns, leading to increased fringe curvature. The interferogram depicted in Fig. 4(b) shows quasi-steady two-dimensional flow patterns in the two-layer system, seen at the end of 6 hours of experimentation.

In the air layer, the flow develops in the form of a single roll. It rises along the left side wall and descends along the right side wall. This gives an unicellular pattern in the cavity with sense of rotation in the clockwise direction. The fringes in the central portion were seen to switch between two states, one comparatively long-lived in relation to the other. The dominant trend in the cavity was captured and is shown in Fig. 4(b). In the water phase, the flow develops in the form of four counter-rotating rolls with upflow close to the cavity center and downflow near sides. The fringes in the central portion were seen to switch among 5-6 states, though only one of them was long-lived. The dominant state was recorded by the camera and is shown in Fig. 4(b). The temperature profiles shown in Fig. 6 indicates large temperature drop in air compared to water. Interface temperature comparison with the reference is shown in Tab. 1. The width-averaged Nusselt number calculated for the cavity walls and the reference values are given in Tab. 2. The experimental and the reference Nusselt numbers appear to be close. However, it should be recalled that significant differences in average Nusselt numbers would be seen if all possible flow states, including the purely transient were included in the calculation. Flow coupling between air and water layers in the present experiment is quite dominant at the interface. Here, a single roll in the air, and four counter-rotating rolls in the water layer have been observed. It was observed that the convection cells in water tend to destabilize the patterns in air, by introducing unsteadiness. There is evidence of a mechanical coupling between the two-layers at the interface. At the same time, the flow fields in individual layers are driven by the respective temperature differences, suggesting the coupling to be thermal in nature. Thus, one may con-

clude that the fluid layers are fully or jointly coupled.

4.3 Flow Characteristics in a Cavity - Thicker Air Layer



(a) (b)

Figure 5 : Steady state interferogram for air-water system having thicker air layer in a square cross-section cavity with a temperature difference of (a) 10 K and (b) 18 K across the cavity

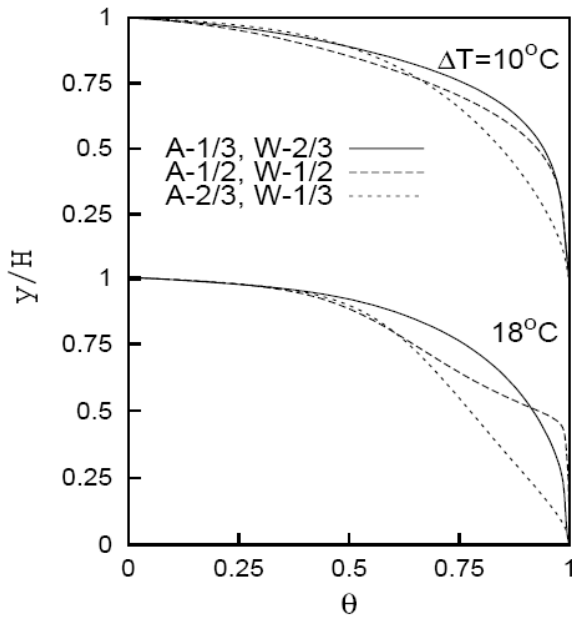


Figure 6 : Width Averaged Temperature Profile for different layer heights of air-water system in a square cross-section cavity with a temperature difference of 10 K and 18 K across the cavity.

In the first case, a temperature difference of 10 K was imposed between the surfaces. The average cavity temperature was 21°C and the interface temperature was found

Table 1 : Comparison of Interface Temperature with reference [3], for different heights of water filled in a square cavity, the rest being air, with varying temperature differences across the cavity, and the corresponding Rayleigh Numbers on the air and water side.

ΔT , K	Layer Heights	T_I , °C	T_I , °C (Reference)
10	A-1/3, W-2/3	25.72	25.80
	A-1/2, W-1/2	25.82	25.79
	A-2/3, W-1/3	24.62	25.81
18	A-1/3, W-2/3	32.30	33.65
	A-1/2, W-1/2	33.72	33.64
	A-2/3, W-1/3	31.21	33.69

to be 25.81°C. This gives the Rayleigh number in air and water to be 9,939 and 4,420 respectively. A more vigorous convective motion is noticed in air than in water due to higher driving buoyancy potential. The flow in the air portion showed high unsteadiness, unlike the water portion; where the flow was quite steady. The flow in air was observed to switch among 2 states. The long lived flow pattern, observed as the dominant mode, was recorded by the camera and is shown in Fig. 5(a). The interferogram depicted in Fig. 5(a) shows quasi-steady two-dimensional flow patterns in the two-layer system. In the air portion of the cavity, the flow develops in the form of a primary roll which rises along the left side wall and descends near the right side wall. A very weak secondary roll was also noticed near the right side wall which rotates counter to the primary roll. In the water phase, the flow develops in the form of a primary roll which rises along the right side wall and descends near the left side wall. Also, a very weak secondary roll was noticed near the left side wall which rotates counter to primary roll. The temperature profiles of isotherms in the air and water sides of the cavity are shown in Fig. 6. The figure shows large temperature drop in air than in water. The interface temperature obtained from the experiments and the reference value are compared in Tab. 1. The width averaged Nusselt number calculated from experiments and the reference values from the correlations are compared in Tab. 2. Flow coupling exists in the present experiment due to convective flow in both the layers. Here, a dominant primary roll in air as well as in water have been observed. In air, the sense of rotation of the roll is in the clockwise direction, which is opposed to water, where it is in the counter-clockwise direction. Thus, it may be

Table 2 : Comparison of Average Nusselt Number with reference [3], at cold (air side) and hot (water side) walls, for different layer heights of water filled in a square cross-section cavity, the rest being air, with varying temperature differences across the cavity.

ΔT , K	Layer Heights	Nu (air)	Nu (ref.)	Nu (water)	Nu (ref.)
10	A-1/3, W-2/3	0.98	1.0	3.21	4.35
	A-1/2, W-1/2	1.96	1.85	2.97	3.68
	A-2/3, W-1/3	2.60	2.38	2.09	2.62
18	A-1/3, W-2/3	1.34	1.27	3.60	5.37
	A-1/2, W-1/2	1.99	2.16	3.70	4.50
	A-2/3, W-1/3	2.53	2.71	3.03	3.32

inferred that the flow in the lower layer is driven by the viscous drag of the upper layer at the interface, suggesting the coupling to be mechanical in nature. Also, at the same time the flow fields in individual layers are driven by the respective temperature differences, suggesting the coupling to be thermal in nature. Thus, it may be concluded that a full (mechanical + thermal) coupling exists at the interface. In the second case, a temperature difference of 18 K was imposed between the surfaces. The average cavity temperature was 25°C and the interface temperature was found to be 33.69°C. Accordingly, the Rayleigh number calculated in air and water to be 16,844 and 10,666 respectively. This gives high driving buoyancy potential in air as compared to water. In this case also, the flow in the air portion showed quite a high unsteadiness in the central portion of the cavity, imparting slight unsteadiness in the water portion, which was otherwise steady. It was observed that the flow in air has reached the Time Dependent regime as discussed by Krishnamurti (1970). The flow in the air portion were seen to switch among two states. The dominant state (long lived state) was recorded by the camera and is shown in Fig. 5(b).

In the air portion of the cavity, the flow develops in the form of a twin counter-rotating rolls with down-flow close to the center and up-flow along the sides of the cavity. In the water phase, the flow develops in the form of four counter-rotating rolls with up-flow close to the cavity center and down-flow near the sides. The temperature profiles of isotherms in the air and water sides of the cavity are shown in Fig. 6. The figure shows large temperature drop in air than in water. The interface temperature obtained from the experiments and its reference value are compared in Tab. 1. Similarly, the width averaged Nusselt number and the correlated value are compared in Tab.

2. Flow coupling exists in the present experiment due to convective flow in both the layers. Here, twin counter-rotating rolls in air, and four counter-rotating rolls in water have been observed. It was observed that down-flow of the upper layer was aligned with up-flow of the lower layer near the cavity center. It indicates the rolls in the two-layers to be oppositely oriented near the cavity center. This indicates the coupling to be mechanical in nature. Also, convective flow in each layer is driven by the individual temperature differences across the respective fluid layers, indicating thermal coupling at the interface. Thus, we conclude that a full (joint) coupling consisting of both thermal and mechanical interactions was present at the interface.

5 Conclusions

Buoyancy-driven convection in a differentially heated cavity containing air and water was experimentally studied, using a Mach-Zehnder interferometer. The flow field was mapped in terms of fringe patterns that were indicative of isotherms in the cavity. Parametric study for three different layer heights of water and air in a rectangular in-plan cavity have been done for analyzing the two-layer convection. Layer heights selected in the square cross-section cavity for the present problem were: (1) 1/3rd Air - 2/3rd Water, (2) 1/2 Air - 1/2 Water, and (3) 2/3rd Air - 1/3rd Water. The following temperature differences for each layer heights were imposed across the hot and cold walls of the cavity: (1) $\Delta T = 10$ K and (ii) $\Delta T = 18$ K. These led to Rayleigh numbers in the range in air and in water. A steady two-dimensional convection pattern was obtained at the lowest Rayleigh number. An increase in the Rayleigh number led to weak unsteadiness in the flow patterns in the air side and strong unsteadiness in the water side. The temperature profile across the

fluid layers clearly indicated a large temperature drop in air compared to the water phase. This suggests the split of temperature drops in the individual fluid layers as the inverse ratio of their respective thermal conductivities. The interface temperature calculated from water side was found to be quite close to that from the air side in all cases. The average Nusselt number for the cavity showed some difference with the reference Nusselt number, the reason being one of the surfaces, namely the interface is not rigid. A passive conductive state i.e. no-flow state was observed in the upper layer owing to Rayleigh number less than the critical value. These led to no-coupling, in thicker water layer case, at lowest Rayleigh number to shift to thermal coupling at higher Rayleigh numbers. As the driving buoyancy potential ratio increases between water and air layers, as in equal layer heights, the flow coupling has changed from thermal mode to full (thermal + mechanical) coupling mode at the interface. For thicker air layer, a full coupling was observed in the cavity, even though the driving buoyancy potential ratio approaches 1.6 with increasing temperature differences between walls.

Acknowledgement: One of the authors (Sunil Punjabi) is grateful to the Quality Improvement Programme (Q.I.P) scheme run by the Ministry of Human Resources Development (H.R.D), Government of India for the financial assistance provided during his doctoral work at the Department of Mechanical Engineering, Indian Institute of Technology (I.I.T) Kanpur 208 016 India.

References

- Andereck, David C.; Colovas, Michael M.; Peter, W.D.** (1996): Observation of time-dependent behaviour in the two-layer Rayleigh-Benard system, *Proceedings of the third Microgravity Fluid Physics Conference*, pp. 313-318.
- Dijkstra, Henk A.** (1992): On the structure of cellular solutions in Rayleigh-Benard-Marangoni flows in small-aspect-ratio containers, *J. Fluid Mechanics*, vol. 243, pp. 73-102.
- Gebhart B.; Jaluria Y.; Mahajan R.L.; Sammakia B.** (1988): *Buoyancy-Induced Flows and Transport*, Hemisphere Publishing Corporation, New York.
- Goldstein R.J.**, (Editor), (1983; second edition 1995): *Fluid Mechanics Measurements*, Hemisphere Publishing Corporation, New York.
- Johnson, D.; Narayanan, R.; Dauby, P.C.** (1999): The effect of Air Height on the pattern formation in Liquid-Air Bilayer Convection, *Fluid Dynamics at Interface*, Cambridge University Press, Cambridge, pp. 15-30.
- Krishnamurti R.** (1970): On the Transition to Turbulent Convection. Part 1: The Transition from Two to Three Dimensional Flow, *Journal of Fluid Mechanics*, vol. 42, part 2, pp. 295-307.
- Lappa M.** (2005): On the nature and structure of possible three-dimensional steady flows in closed and open parallelepipedic and cubical containers under different heating conditions and driving forces, *FDMP: Fluid Dynamics and Materials Processing*, vol. 1, no. 1, pp. 1-19.
- Mishra, D.; Muralidhar, K.; Munshi, P.** (1999): Interferometric study of Rayleigh-Benard Convection using Tomography with limited projection data, *Experimental Heat Transfer*, vol. 12, pp. 117-136.
- Mosaad, M.; -Nakhi, A.B.; Al-Hajeri, M.H.** (2005): Thermal communication between two vertical systems of free and forced convection via heat conduction across a separating wall, *FDMP: Fluid Dynamics and Materials Processing*, vol. 1, no. 4, pp. 301-313.
- Prakash, A.; Koster, J.N.** (1996): Steady Rayleigh-Benard Convection in a Two-Layer system of Immiscible liquids, *Transactions of the ASME, J. Heat Transfer*, vol. 118, pp. 366-373.
- Punjabi, S.; Muralidhar, K.; Panigrahi, P.K.** (2004): Buoyancy-driven convection in two superposed layers in an octagonal cavity, *International Journal of Thermal Sciences*, vol. 43, pp. 849-864.
- Rasnat, S.; Busse, F.H.; Rehberg, I.** (1989): A theoretical and experimental study of double-layer convection, *J. Fluid Mechanics*, vol. 199, pp. 519-540.
- Schatz, M.F.; VanHook, S.J.; McCormick, W.D.; Swift, J.B.; Swinney, H.L.** (1999): Time-independent square patterns in surface-tension-driven Benard convection, *Physics of Fluids*, vol. 11, no. 9, pp. 2577-2582.
- Zeren, R.W.; Reynolds, W.C.** (1972): Thermal instabilities in two-fluid horizontal layers, *J. Fluid Mechanics*, vol. 53, no. 2, pp. 305-327.

